symmetry

MDPI

Article

Identification of Retained Austenite in 9Cr-1.4W-0.06Ta-0.12C Reduced Activation Ferritic Martensitic Steel

Rengachari Mythili [1,2,*], Ravi Kirana [3], Loushambam Herojit Singh [4], Ramanujam Govindaraj [2,5], Anil K. Sinha [6], Manvendra N. Singh [7], Saibaba Saroja [1,†], Muraleedharan Vijayalakshmi [1,†] and Sudip K. Deb [7]

1 Metallurgy & Materials Group, Indira Gandhi Centre for Atomic Research, Kalpakkam 603102, India; saroja.saibaba@gmail.com (S.S.); vijayalakshmi.muraleedharan@gmail.com (M.V.)
2 Homi Bhabha National Institute at IGCAR, Kalpakkam 603102, India; govind@igcar.gov.in
3 Department of Physics and Nanotechnology, SRM Institute of Science and Technology, Kattankulathur 603203, India; ravikirs@srmist.edu.in
4 Department of Physics, NIT Manipur, Langol 795004, India; herojit@nitmanipur.ac.in
5 Materials Science Group, Indira Gandhi Centre for Atomic Research, Kalpakkam 603102, India
6 Department of Physics, University of Petroleum and Energy Studies, Dehradun 248007, India; anil.sinha@ddn.upes.ac.in
7 Raja Ramanna Centre for Advanced Technology, Indore 452013, India; manavendra@rrcat.gov.in (M.N.S.); skdeb@rrcat.gov.in (S.K.D.)
* Correspondence: rm@igcar.gov.in
† These authors have superannuated.

Abstract: Reduced activation ferritic martensitic (RAFM) 9Cr steels, which are candidate materials for the test blanket module (TBM) of nuclear fusion reactors, are considered to be air hardenable. However, alloy composition and the processing conditions play a significant role during the transformation of austenite to martensite/ferrite on cooling. The presence of retained austenite is known to influence the mechanical properties of the steel. Identifying very low amounts of retained austenite is very challenging though conventional microscopy. This paper aims at identifying a low amount of retained austenite in normalized 9Cr-1.4W-0.06Ta-0.12C RAFM steel using synchrotron X-ray diffraction and Mossbauer spectroscopy and confirmed by advanced automated crystal orientation mapping in transmission electron microscopy. Homogeneity of austenite has been understood to influence the microstructure of the normalized steel, which is discussed in detail.

Keywords: reduced activation ferritic martensitic steel; microstructure; martensite; retained austenite; automated crystal orientation mapping-transmission electron microscopy; Mossbauer spectroscopy

Citation: Mythili, R.; Kirana, R.; Singh, L.H.; Govindaraj, R.; Sinha, A.K.; Singh, M.N.; Saroja, S.; Vijayalakshmi, M.; Deb, S.K. Identification of Retained Austenite in 9Cr-1.4W-0.06Ta-0.12C Reduced Activation Ferritic Martensitic Steel. *Symmetry* **2022**, *14*, 196. https://doi.org/10.3390/sym14020196

Academic Editors: Partha Pratim Das, Arturo Ponce-Pedraza, Enrico Mugnaioli and Stavros Nicolopoulos

Received: 27 October 2021
Accepted: 15 December 2021
Published: 20 January 2022

1. Introduction

Reduced activation ferritic martensitic (RAFM) 9Cr steels are considered to be candidate materials for test blanket module (TBM) for nuclear fusion reactors, due to their excellent mechanical properties [1–3]. They are also a very good structural materials for steam generator circuits [4,5] as they exhibit good thermal conductivity and low thermal expansion coefficient [6,7].

The 9Cr ferritic/martensitic steels are reported to be air hardenable [8], after normalization above Ac_3 temperature. These steels with a low carbon content (<0.15%) are known to form a lath martensitic structure with a dislocation substructure [9,10]. Though martensite gives good strength to the steel, due to limited ductility, these steels are not recommended to be used in normalized condition [11,12]. Therefore, the steels are generally used in the normalized and tempered condition with a tempered martensitic structure possessing good mechanical properties. However, preceding the tempering treatment, normalizing the steel in the single austenite phase is also an essential step for the transformation to a complete martensitic structure [11–13]. The decomposition of austenite is known to be influenced by the rate of cooling (Q) from the austenitizing temperature and the alloy chemistry [11,12].

Continuous cooling transformation (CCT) and time temperature transformation (TTT) of 9 Cr steels have been already studied [10,14]. As per the existing literature, CCT or TTT diagrams explain the presence of martensite/ferrite and carbides depending on the cooling rates adopted, but not the presence of retained austenite in 9Cr ferritic steels [9–12]. Martensitic transformation of austenite is well known to be accompanied by strain dictated by the composition of the steel and the cooling rates and hence the transformation induced strain can induce the mechanical stabilization of the austenite, and the mechanical stability of retained austenite is important in obtaining good toughness [15]. In fact, residual stress introduced unintentionally in weldments during fabrication can augment the transformation strain that could impede complete martensitic transformation of austenite. It is reported that mechanical stabilization might play an even greater role for retained austenite in the weldments of modified 9Cr–1Mo steel, which exhibits higher creep strength than most low alloy steels [15]. Santella et al. [16] report an incomplete austenite transformation in the weld metal of modified 9Cr-1Mo steel during initial cooling from an austenitizing treatment and the transformation of retained austenite to martensite during tempering, and attributed to the effects of microsegregation. The presence of retained austenite can be undesirable in the steel, if it is metastable, and can lead to the formation of untempered martensite or inhomogeneity after tempering [17]. Inhomogeneity in such steel components can have a significant negative impact on the mechanical properties, reducing the service life. During tempering, decomposition of retained austenite to different carbides is influenced by tempering temperature and time, which in turn, are responsible for temper embrittlement of the steel [18,19]. Therefore, it is pertinent to identify the reasons for the presence of retained austenite in such steels and also characterize using appropriate techniques, since the amount of retained austenite could be very low. Hence, in this study, a detailed microstructural characterization of RAFM steel in normalized as well as tempered condition has been taken up, to understand the decomposition mode of high temperature austenite.

2. Materials and Methods

The steel used in the present study is designated at INRAFM steel and the chemical composition of the steel is given in Table 1. The steel was subjected to austenisation at 1253 K for 30 min and subjected to air cooling (normalizing). The normalized steel was also tempered at 1033 K for 1 h.

Table 1. Chemical composition of INRAFM steel (wt%).

Element	Concentration	Element	Concentration
Cr	9.03	**Ta**	0.06
C	0.126	**N**	0.03
Mn	0.56	**O**	0.002
V	0.24	**P**	<0.002
W	1.38	**S**	<0.001

Preliminary microstructural analysis was carried out in scanning electron microscope (Philips XL30, F.E.I. Company: Hillsboro, OR, USA). Angle dispersive X-ray diffraction (ADXRD) experiments were carried out using beam line (BL-12) at an Indian synchrotron source (Indus 2), at Raja Ramanna Centre for Advanced Technology (RRCAT), Indore, since the high brilliance of synchrotron source compared to conventional source would enable the identification of phases of volume fraction less than 1%. A monochromatic X-ray beam ($\lambda/\Delta\lambda$ = 8000 at ~8 keV) of photon energy 13.081 KeV (λ = 0.9478 A°) or 16 keV and beam size 300 × 300 μm^2 was used. NIST LaB_6 powder was used for calibration of wavelength in transmission mode. Synchrotron XRD experiments were carried out on thin foils of the steels (~100 μm thick) in the transmission mode using MAR Research image plate (MAR 345 DTB). Image plate data was converted to I vs. 2 θ plot using FIT2D software. Mossbauer spectroscopy was carried out on thin foils (~100 μm thick) of the steels, with Co^{57} source

dispersed in Rh matrix as the probe with a Wiesel spectrometer in transmission geometry. Thin foil specimens for TEM were prepared by conventional mechanical thinning followed by electrolytic polishing with a Struers jet thinning apparatus (Tenupol-5) with appropriate electrolyte, while carbon extraction replica specimens were prepared by picking up the thin film of carbon deposited on the steel surface immersed in Villela's reagent followed by rinsing in methanol transmission electron microscopy observations were carried out with Philips CM200 analytical transmission electron microscopy (ATEM) at an acceleration voltage of 200 kV. EDX analysis was carried out with the Oxford EDS system attached to the ATEM. Orientation imaging in TEM was carried out with an automated crystal orientation mapping (ACOM) system from M/s. Nanomegas SPRL, Brussels, Belgium.

3. Results

Secondary electron (SE) and back scattered electron (BSE) images of the normalized steel are shown in Figure 1a,b. It is observed that the structure is martensitic in the normalized steel. Presence of undissolved primary carbides is also observed in the normalized steel from Figure 1b. Detailed selected area diffraction (SAD) and energy dispersive X-ray (EDX) analysis of the precipitates seen in TEM micrograph in Figure 1c confirmed that the precipitates are Cr, W rich $M_{23}C_6$ and Ta, V rich MX as shown in Figure 1d. In addition, the presence of fine, acicular carbides has been noted in a few wide laths of the normalized steel (Figure 2a), which were identified to be Fe rich M_3C carbides as shown in Figure 2b,c.

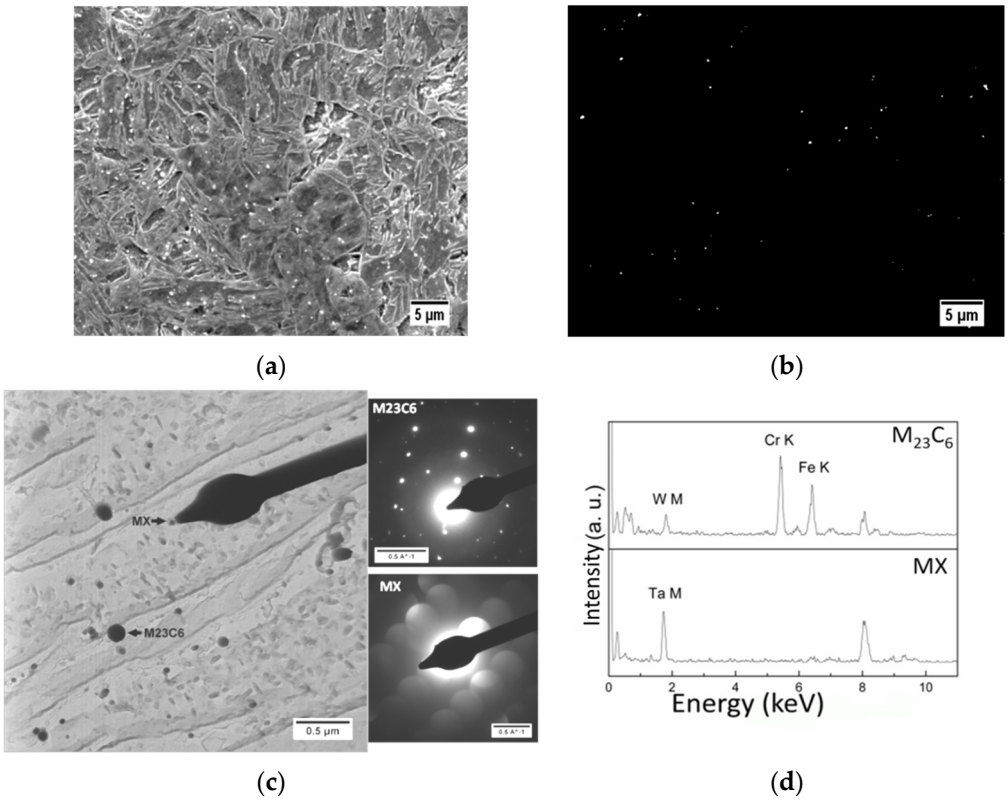

Figure 1. Microstructure of 1.4W-0.06Ta steel normalized at 1253 K: (**a**) SE image showing martensite; (**b**) BSE image showing undissolved carbides; (**c**) carbon extraction replica BF image along with diffraction patterns from $M_{23}C_6$ and MX along $[5\,4\,\bar{5}]$ and $[\bar{1}\,1\,2]$ zone axis respectively; (**d**) EDX spectra from undissolved $M_{23}C_6$ and MX carbides.

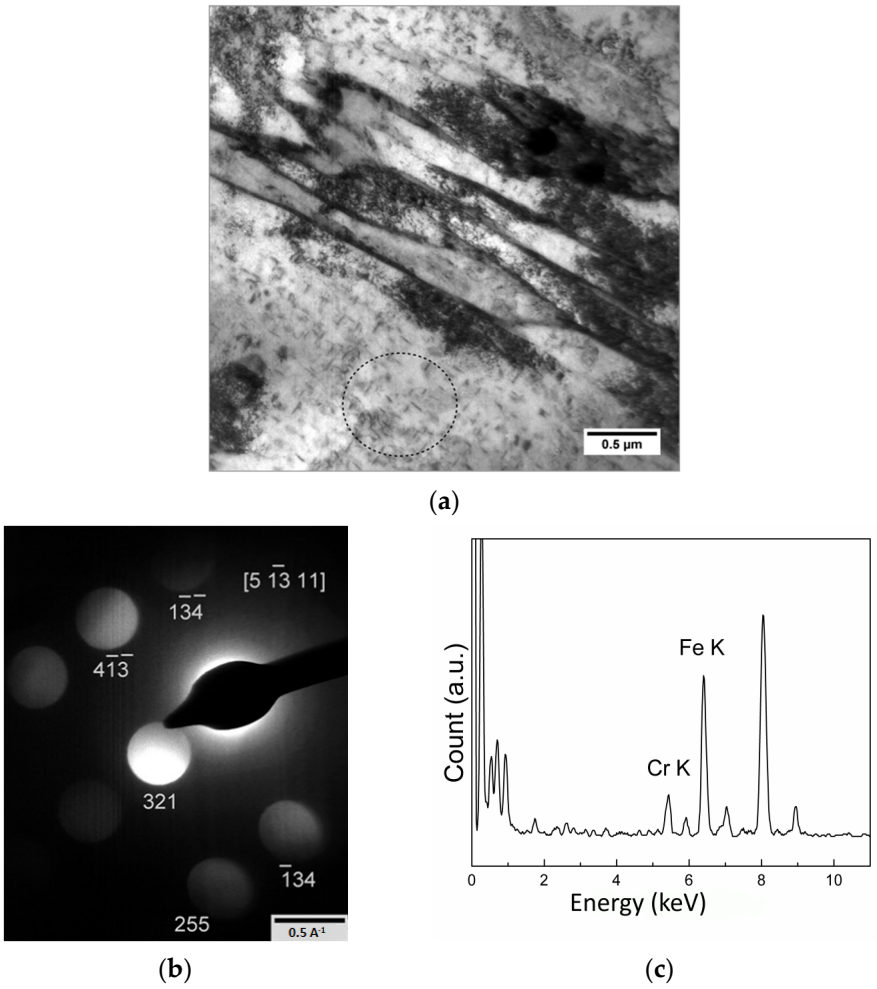

Figure 2. (**a**) Bright field image of normalised1.4W-0.06Ta steel showing fine carbides (circled) in a wide lath; (**b**) micro diffraction pattern from a precipitate along -$[5\ \bar{1}3\ 11]$ zone axis of M_3C; (**c**) typical EDS spectrum of these carbides from carbon extraction replica of the same sample, showing Fe enrichment.

Microstructural features of the normalized and tempered steel are shown in Figure 3a–d. It is observed that the microstructure is tempered martensite with the presence of higher amounts of Cr rich $M_{23}C_6$ at the boundaries of prior austenite grains and martensitic laths and intralath MX precipitates enriched with Ta, V, which is in agreement with results available in literature on these steels [14]. However, contrary to the presence of Fe rich M_3C in the normalized steel, no signature for M_3C could be found in the tempered steel. This suggests the metastable nature of M_3C.

Conventional laboratory XRD spectra of the normalized as well as normalized and tempered steels showed the presence only α-bcc peaks, corresponding to the martensite/ferrite matrix, due to the low amounts of precipitates in the tempered steel. Methods such as electrolytic phase extraction can enable the identification of low amounts secondary phases with the matrix interference even by laboratory X-ray sources [20] or alternatively, synchrotron XRD is well known to be suitable for phase identification with low detection limits [21]. ADXRD spectra of the normalized as well as the tempered steels are presented in Figure 4a. Since the carbon concentration of the steel used in the present study is low, it is assumed that the lattice parameter of martensite is not significantly different from BCC α-Fe. Apart from the major phase α-Fe, peaks corresponding to the secondary phases $M_{23}C_6$ and MX precipitates could also be indexed. However, the intensity ratio of the peaks did not follow the JCPDS data, due to certain experimental difficulties such as static nature of the sample, intensity saturation of the image plate, etc. In the ADXRD spectrum

of the normalized steel, (Figure 4b), the (110)α peak of highest intensity is asymmetrical and could be resolved into two peaks, the one with a lower intensity identified as (111) peak of austenite. The other peaks of austenite could not be unambiguously indexed, since they were overlapping with that of the undissolved $M_{23}C_6$ and MX precipitates. On the other hand, in the normalized and tempered steel, such a deconvolution of $(110)_\alpha$ peak was not possible, which clearly indicates the absence of austenite after tempering.

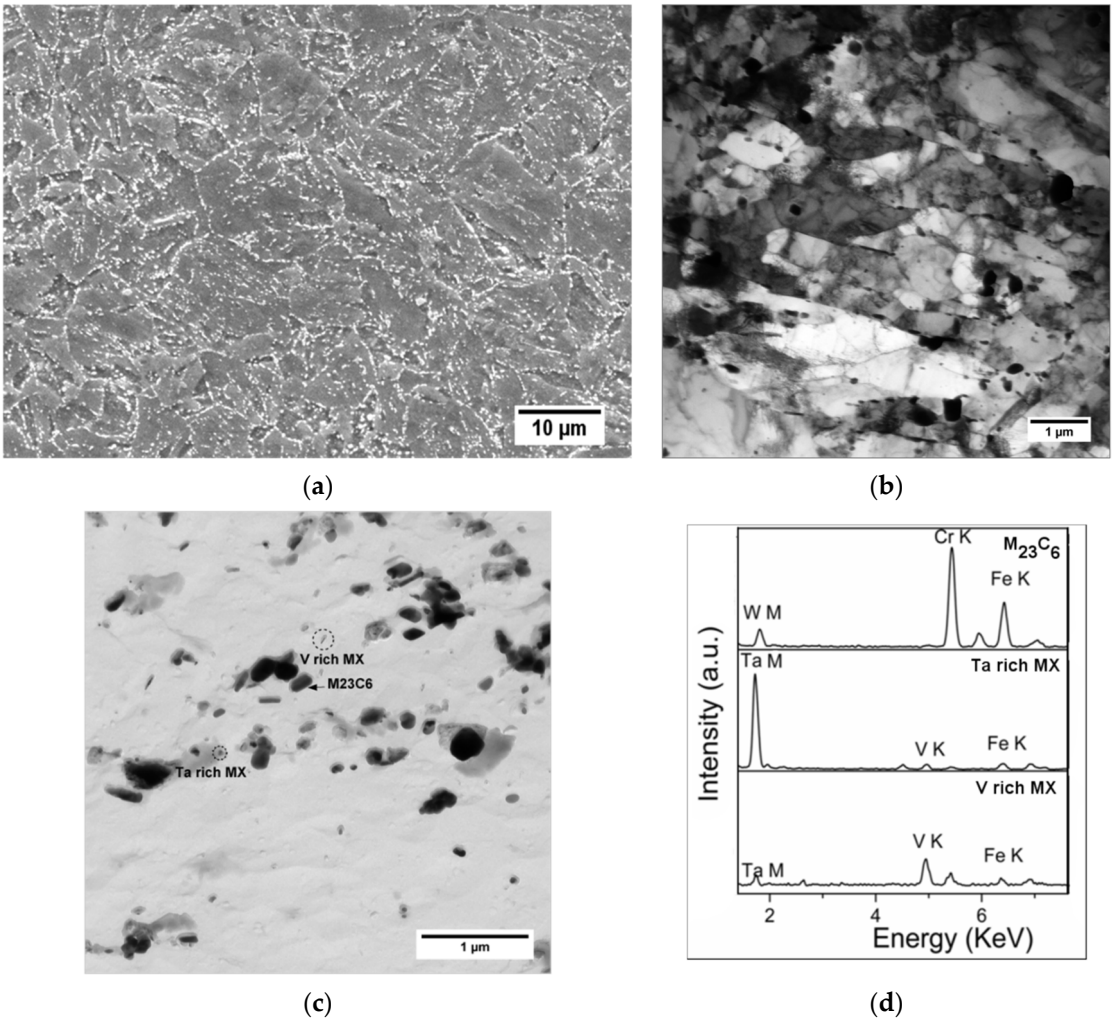

Figure 3. Microstructure of normalised and tempered 1.4W-0.06Ta steel showing tempered martensite: (**a**) SE image showing extensive precipitation of carbides along PAGB and lath boundaries; (**b**,**c**) TEM micrographs showing interlath $M_{23}C_6$, intra lath MX precipitates; (**d**) EDX spectra from Cr rich $M_{23}C_6$ carbides and Ta, V rich MX precipitates.

Figure 5a,b shows the Mossbauer spectra of normalized as well as normalized and tempered steels. It is observed that the steel in both the conditions exhibit a six-line pattern, which could be further resolved into three six-line patterns. Such resolved components are due to a complex interplay of the alloying elements, which is beyond the scope of this study. The presence of a six-line pattern is mainly attributed to the predominant ferro magnetic bcc ferrite. Interestingly, in the normalized steel, in addition to the six-line patterns, spectrum could be deconvoluted to show the presence of a single line pattern of low intensity (arrow marked in Figure 5a). Such a singlet clearly suggests the presence of a non-magnetic cubic phase, which could be retained austenite or the undissolved $M_{23}C_6$ and MX precipitates, since all these phases are known to possess a fcc structure and also paramagnetic. However, no such singlet was observed in the normalized and tempered steel, where the amount of $M_{23}C_6$ and MX precipitates, is higher than in the normalized steel. Hence, the singlet

observed in the normalized steel should correspond to retained austenite of a low volume fraction [9,22] rather than due to the presence of undissolved carbides.

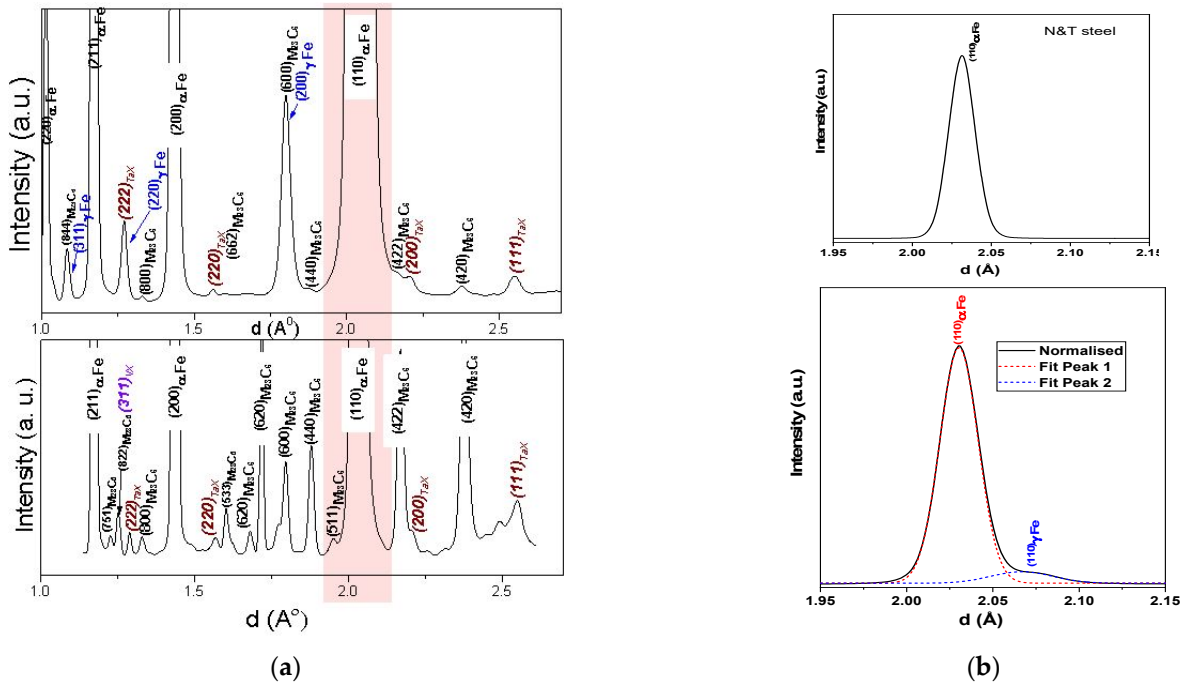

Figure 4. (**a**) ADXRD spectra of Normalised and normalised and tempered steel showing different phases; (**b**) (110) peak of ferrite (BCC) and (111) peak of austenite (FCC) phases resolved in normalised steel (top) after deconvolution; (110) peak of ferrite (BCC) in normalised and tempered steel.

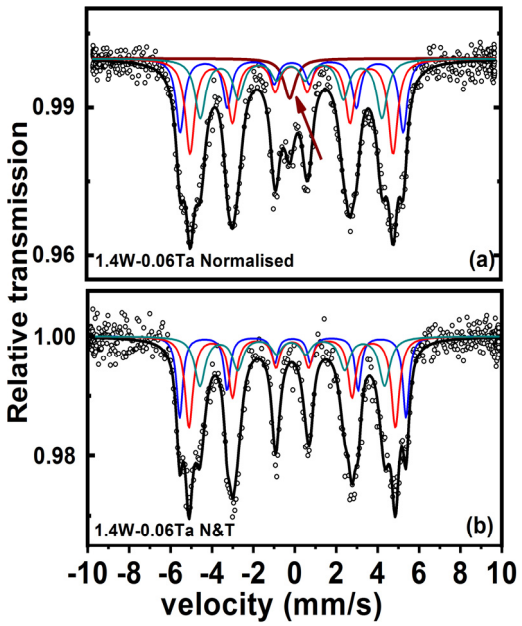

Figure 5. Mossbauer spectra of the 1.4W-0.06Ta steel in: (**a**) normalized condition showing the presence of a single line pattern (arrow marked) due to low amount of retained austenite in addition to six-line pattern due to ferromagnetic ordering; (**b**) normalized and tempered condition (bottom) showing only ferromagnetic ordering.

Conventional TEM observations could not unambiguously confirm the presence of retained austenite in the normalized steel. Hence a newly emerging technique automated crystal orientation mapping in TEM (ACOM-TEM), was employed. Crystallographic data

for α ferrite, γ austenite and $M_{23}C_6$ were given as input for analysis. Figure 6a,b shows the resultant index and reliability maps of the normalized steel, while Figure 6c shows the orientation map from the same region. Multiple orientation of martensite is quite evident from Figure 6c, which can be attributed to a fast-cooling rate adopted during normalizing. The phase map presented in Figure 6d showed the presence of ~2% retained austenite.

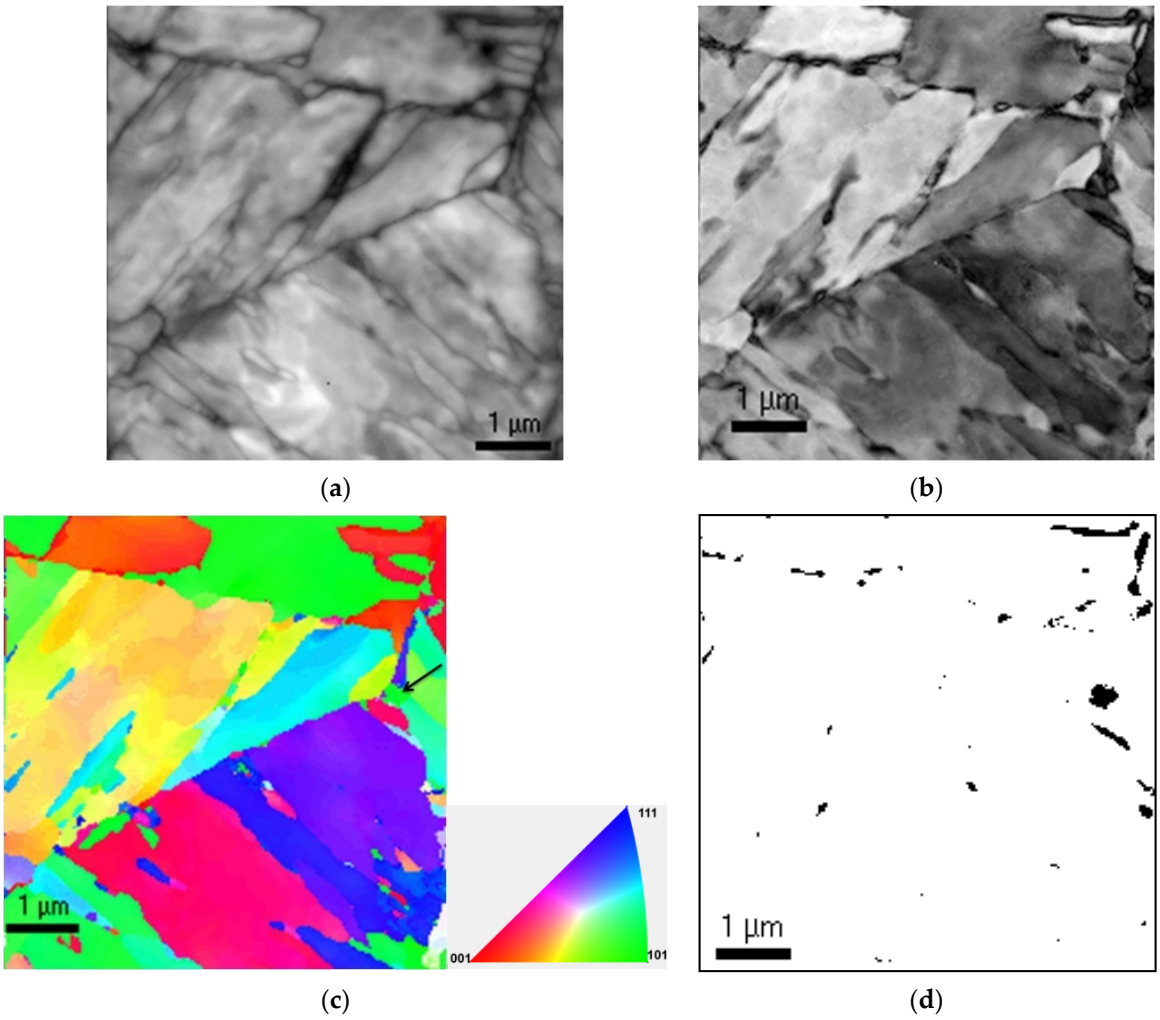

Figure 6. Orientation imaging of normalized 1.4W-0.06Ta steel showing: (**a**) index map; (**b**) reliability map; (**c**) orientation map showing random orientation of martensite laths; (**d**) phase map showing retained γ.

4. Discussion

Formation of martensite in 9Cr ferritic/martensitic steels air cooled at the rate of ~2 K/min is well reported [23]. Transformation of Fe from FCC to BCC is known to follow the Bain, Kurdjumov–Sachs (K-S), Nishiyama–Wassermann (N-W) or Greninger–Troiano (G-T) orientation relationship (OR) [24]. K-S and N-W OR are more frequently reported in low C steels. However, the more common factors, which can influence on OR are thermo-mechanical processing and chemical composition [24,25]. In low carbon ferritic/martensitic steels, $\gamma \rightarrow \alpha'$ transformation reportedly follows K-S OR [26,27],which can result in 24 crystallographic variants of α from a given γ orientation. Hence in this study also, it is expected that martensite forms obeying the K-S OR.

From Figure 6c, it is clearly observed that several orientations of the packets of martensite nucleated from the 4 {111} planes of γ as indicated by the legend in Figure 6c, the standard stereographic triangle of a cubic system. The observation of many orientations

within each austenite grain suggests that there is no variant selection, which is due to a relatively fast cooling rate adopted.

Retained austenite in modified 9Cr-1Mo weldments is reported to obey both K-S and N-W orientation relationship [15]. However, Duanjun Sun et al. [28] observe that even when the amount of retained austenite is less, there can be a deviation in the orientation of austenite above M_s, which may be inevitable as a result of strain associated with martensitic transformation. It is reported that thin films of retained austenite between laths of low alloy martensite are mechanically stabilized at the austenite-martensite interface by transformation induced accommodation defects [15]. However, a high degree of mutual accommodation of transformation strains between adjacent variants of martensite with a K-S orientation relationship such as in twin related martensite can suppress the retention of inter-lath austenite [29]. Hence, the observation of retained austenite along with martensite in the normalized steel without any variant selection of martensite in this study could be attributed to its mechanical stabilization associated with the transformation strain.

It is known that γ to α' transformation is significantly influenced by factors such as (a) cooling rate, (b) alloying additions, and (c) homogeneity of austenite. An earlier study of differential scanning calorimetry analysis of this steel austenitized and cooled at different rates clearly showed that at cooling rates less than 40 K/min, there is a cooling rate dependence of the M_s and M_f temperatures [30], with M_s and M_f temperatures decreasing with increase in cooling rate. In addition, it is known both M_s and M_f temperatures decrease with the addition of ferrite stabilizers W and Ta, which are also strong carbide formers [6]. The dissolution temperature of $M_{23}C_6$ and MX precipitates in this steel was determined to be higher than 1342 and 1570 K respectively [30]. Hence, in this steel with 1.4% W, it can be inferred that normalizing at 1253 K is insufficient for complete dissolution of these carbides as shown in Figure 1. Such incomplete dissolution of the primary carbides can lead to the inhomogeneity of the austenite, which would increase with W or Ta content of the steel [12]. Further detailed analysis of martensitic lath structure in TEM showed two different types of lath structure [12]. Such a precipitation of Fe rich M_3C was shown to occur in a few wide laths, while the laths with narrow width showed no precipitation. This had been understood to be due to the inhomogeneous austenite around the undissolved carbides—one lean w.r.t carbon and the other enriched with carbon, since it is known that carbon migration is possible even at lower temperatures also [31]. Carbon lean austenite has a relatively higher M_s and M_f temperatures leading to the partial transformation of γ to α + *carbides* (similar to bainite) above M_s, [12,32] as shown in Figure 2. Variation in lath size and the carbide precipitation indicates that the stability of the inhomogeneous austenite is influenced by the cooling rate. The observation of the austenite in the normalized steel has been unambiguously confirmed by various experimental techniques, which could be due to an incomplete martensitic transformation of the carbon enriched austenite. Presence of retained austenite as thin films at martensitic lath boundaries in the weldments of this class of steels has been reported in literature [33]. Hence the transformation sequence of the steel during normalizing can be summarized as

Austenite + undissolved carbides $\rightarrow$ *martensite* (α') + α + *carbides* + *traces of retained austenite* (γ_r)

Absence of Fe rich carbides in the tempered steel proves that the M_3C present after normalization is unstable. It is well reported that the stable carbides in these steels after tempering in the temperature range of 750–780 °C are $M_{23}C_6$ and MX [18,34]. In addition, no signature of austenite could be found in the tempered steel. Hence, it can be inferred that the observed microstructure containing *martensite* + α + *carbides* + γ_r is due to the complex interplay of micro chemical variation/inhomogeneity in the alloy even after normalizing at 1253 K for 30 min. This is also attributed to the sluggish diffusion of heavy elements such as W and Ta [35] in the steel. Further to support the fact of sluggish kinetics, it is reported in an earlier work that the number density of carbides in the steel increases with increase in W content [36].

5. Conclusions

Microstructural investigation on 9Cr-1.4W-0.12C Ferritic martensitic steel was performed in the present work. The salient results of the study are as follows:

- Conventional TEM analysis of normalized steel shows a martensitic structure with few wide laths containing Fe rich M_3C carbides;
- Detailed analysis of ADXRD, orientation imaging in TEM and Mossbauer studies proved the presence of retained austenite in normalised steel;
- The presence of M_3C and retained austenite in the normalized steel with a martensitic microstructure is understood to be due to the inhomogeneity of austenite with incomplete dissolution of primary carbides during normalizing treatment;
- Absence of retained austenite and M_3C in the tempered steel suggested their metastable nature, which could have transformed to stable $M_{23}C_6$ and MX precipitates on tempering.

Author Contributions: Conceptualization, methodology, R.M., S.S. and M.V.; data curation, formal analysis, investigation, R.M., R.K., L.H.S., R.G., M.N.S. and A.K.S.; writing—original draft preparation, R.M., R.K. and S.S.; writing—review and editing, R.M., R.K., S.S. and R.G.; project administration, S.S., M.V., S.K.D. All authors have read and agreed to the published version of the manuscript.

Funding: This research received no external funding.

Institutional Review Board Statement: Not applicable.

Informed Consent Statement: Not applicable.

Data Availability Statement: The data that support the findings of this study are not available at present, as it is a part of the ongoing research.

Acknowledgments: The authors wish to thank Arup Dasgupta, Physical Metallurgy Division, S. Raju, Metallurgy and Materials Group and B. Venkatraman, Indira Gandhi Centre for Atomic Research for their encouragement and support during this work.

Conflicts of Interest: The authors declare no conflict of interest.

References

1. Klueh, R.L. Elevated temperature ferritic and martensitic steels and their application to future nuclear reactors. *Int. Mater. Rev.* **2005**, *50*, 287–310. [CrossRef]
2. Harries, D.R. *High-Chromium Ferritic and Martensitic Steels for Nuclear Applications*; ASTM: West Conshohocken, PA, USA, 2001.
3. Abe, F. Precipitate design for creep strengthening of 9% Cr tempered martensitic steel for ultra-supercritical power plants. *Sci. Technol. Adv. Mater.* **2008**, *9*. [CrossRef]
4. Asada, Y.; Dozaki, K.; Ueta, M.; Ichimiya, M.; Mori, K.; Taguchi, K.; Kitagawa, M.; Nishida, T.; Sakon, T.; Sukekawa, M. Exploratory research on creep and fatigue properties of 9Cr-steels for the steam generator of an FBR. *Nucl. Eng. Des.* **1993**, *139*, 269–275. [CrossRef]
5. Zhu, L.; Liu, X.; Fan, P.; Liu, J. A Study of Microstructure Evolution During Creep of 9Cr-1Mo Steel Using Ultrasonic and Hardness Measurements. *J. Mater. Eng. Perform.* **2019**, *28*, 2348–2355. [CrossRef]
6. Li, X.; Yan, Q.; Ma, R.; Wang, H.; Ge, C. First results of characterization of 9Cr-3WVTiTaN low activation ferritic/martensitic steel. *J. Iron Steel Res. Int.* **2010**, *17*, 57–62. [CrossRef]
7. Gao, Y.; Wang, Z.; Liu, Y.; Li, W.; Liu, C.; Li, H. Diffusion Bonding of 9Cr Martensitic/Ferritic Heat-Resistant Steels with an Electrodeposited Ni Interlayer. *Metals* **2018**, *8*, 1012. [CrossRef]
8. Kim, T.K.; Kim, S.H.; Lee, B. Effects of an intermediate heat treatment during a cold rolling on the tensile strength of a 9Cr-2W steel. *Ann. Nucl. Energy* **2009**, *36*, 1103–1107. [CrossRef]
9. Besoky, J.I.; Danon, C.A.; Ramos, C.P. Retained austenite phase detected by Mössbauer spectroscopy in ASTM A335 P91 steel submitted to continuous cooling cycles. *J. Mater. Res. Technol.* **2019**, *8*, 1888–1896. [CrossRef]
10. Wu, Q.S.; Zheng, S.H.; Huang, Q.Y.; Liu, S.J.; Han, Y.Y. Continuous cooling transformation behaviors of CLAM steel. *J. Nucl. Mater.* **2013**, *442*, S67–S70. [CrossRef]
11. Ni, M.; Wang, J.; Liu, J.; Wang, X.; Zhang, K.; Du, C. Microstructure and Mechanical Properties of P91 Steel during Heat Treatment: The Effect of the Cooling Speed during the Normalization Stage. *J. Mater. Eng. Perform.* **2012**, *30*, 2329–2340. [CrossRef]
12. Ravikirana Mythili, R.; Raju, S.; Saroja, S.; Jayakumar, T.; Rajendra Kumar, E. Decomposition modes of austenite in 9Cr-W-V-Ta reduced activation ferritic-martensitic steels. *Mater. Sci. Technol.* **2015**, *31*, 448–459. [CrossRef]

13. Tan, L.; Hoelzer, D.T.; Busby, J.T.; Sokolov, M.A.; Klueh, R.L. Microstructure control for high strength 9Cr ferritic—Martensitic steels. *J. Nucl. Mater.* **2012**, *422*, 45–50. [CrossRef]
14. Haarmann, K.; Vaillant, J.; Bendick, W.; Arbab, A. *The T91/P91 Book*; Vallourec Mannesmann Tubes: Duesseldorf, Germany, 2002; p. 69.
15. Shiue, R.K.; Lan, K.C.; Chen, C. Toughness and Austenite Stability Of Modified 9Cr-1Mo welds after tempering. *Mater. Sci. Eng. A* **2000**, *287*, 10–16. [CrossRef]
16. Santella, M.L.; Babu, S.S.; Swindeman, R.W.; Specht, E.D. In-situ characterization of austenite to martensite decomposition in 9Cr-1Mo-V steel welds. In Proceedings of the Materials Science and Technology 2003 Meeting, Chicago, IL, USA, 9–12 November 2003; pp. 247–256.
17. Ning, B.; Zhou, X.; Shi, Q.; Liu, Y.; Zhao, J.; Zhang, Z. Relationship between austenite stability and martensite formation in modified 9Cr-1Mo steel. *Int. J. Mater. Res.* **2014**, *105*, 232–239. [CrossRef]
18. Fedorova, I.; Kostka, A.; Tkachev, E.; Belyakov, A.; Kaibyshev, R. Tempering behavior of a low nitrogen boron-added 9%Cr steel. *Mater. Sci. Eng. A* **2016**, *662*, 443–455. [CrossRef]
19. Zhang, Y.; Gu, J.; Han, L.; Shen, G.; Li, C. Thermal decomposition characteristics of retained austenite and its influence on impact toughness of B-containing 9Cr1Mo1Co(FB2) steel during the two-step tempering. *J. Mater. Res. Technol.* **2021**, *12*, 2462–2475. [CrossRef]
20. Gao, Q.; Zhang, Y.; Zhang, H.; Li, H.; Qu, F.; Han, J.; Lu, C.; Wu, B.; Lu, Y.; Ma, Y. Precipitates and Particles Coarsening of 9Cr-1.7W-0.4Mo-Co Ferritic Heat-Resistant Steel after Isothermal Aging. *Sci. Rep.* **2017**, *7*, 5859. [CrossRef] [PubMed]
21. Suwanpinij, P. The Synchrotron Radiation for Steel Research. *Adv. Mater. Sci. Eng.* **2016**, *2016*, 2479345. [CrossRef]
22. Carrizo, D.A.; Besoky, J.I.; Luppo, M.; Danon, C.; Ramos, C.P. Characterization of an ASTM A335 P91 ferritic-martensitic steel after continuous cooling cycles at moderate rates. *J. Mater. Res. Technol.* **2019**, *8*, 923–934. [CrossRef]
23. Saroja, S.; Vijayalakshmi, M.; Raghunathan, V.S. Influence of solution treatment on the microstructure of a 9wt.%Cr-lwt.%Mo-0.07wt.%C steel. *Mater. Sci. Eng. A* **1992**, *154*, 59–67. [CrossRef]
24. Suikkanen, P.P.; Cayron, C.; DeArdo, A.J.; Karjalainen, L.P. Crystallographic analysis of martensite in 0.2C-2.0Mn-1.5Si-0.6Cr steel using EBSD. *J. Mater. Sci. Technol.* **2011**, *27*, 920–930. [CrossRef]
25. Kwon, E.P.; Fujieda, S.; Shinoda, K.; Suzuki, S. Martensitic transformation and texture in novel bcc Fe-Mn-Al-Ni-Cr alloys. *Procedia Eng.* **2011**, *10*, 2214–2219. [CrossRef]
26. Dash, M.K.; Karthikeyan, T.; Saroja, S.; Vijayalakshmi, M. Restitution of prior-austenite grain orientation by microtexture analysis of tempered martensite structure in 9Cr-1Mo ferritic steel. *Mater. Sci. Forum* **2012**, *702–703*, 880–883. [CrossRef]
27. Kitahara, H.; Ueji, R.; Tsuji, N.; Minamino, Y. Crystallographic features of lath martensite in low-carbon steel. *Acta Mater.* **2006**, *54*, 1279–1288. [CrossRef]
28. Sun, D.; Li, C.; Xue, X.; Liu, Y.; Guo, Z.; Gu, J. Optimization scheme of the orientation relationship from crystallographic statistics of variants and its application to lath martensite. *Mater. Des.* **2020**, *195*, 109022. [CrossRef]
29. Bhadeshia, H.K.D.H. Theory and Significance of Retained Austenite in Steels. Ph.D. Thesis, University of Cambridge, Cambridge, UK, March 1980.
30. Kirana, R.; Raju, S.; Mythili, R.; Saibaba, S.; Jayakumar, T.; Rajendra Kumar, E. High-Temperature Phase Stability of 9Cr-W-Ta-V-C Based Reduced Activation Ferritic-Martensitic (RAFM) Steels: Effect of W and Ta Additions. *Steel Res. Int.* **2015**, *86*, 825–840. [CrossRef]
31. Speer, J.; Matlock, D.K.; De Cooman, B.C.; Schroth, J.G. Carbon partitioning into austenite after martensite transformation. *Acta Mater.* **2003**, *51*, 2611–2622. [CrossRef]
32. Liu, C.; Zhang, D.; Liu, Y.; Wang, Q.; Yan, Z. Investigation on the precipitation behavior of M3C phase in T91 ferritic steels. *Nucl. Eng. Des.* **2011**, *241*, 2411–2415. [CrossRef]
33. Shirane, T.; Tsukamoto, S.; Tsuzaki, K.; Adachi, Y.; Hanamura, T.; Shimizu, M.; Abe, F. Ferrite to austenite reverse transformation process in B containing 9%Cr heat resistant steel HAZ. *Sci. Technol. Weld. Join.* **2009**, *14*, 698–707. [CrossRef]
34. Kipelova, A.Y.; Belyakov, A.N.; Skorobogatykh, V.N.; Shchenkova, I.A.; Kaibyshev, R.O. Tempering induced structual changes in steel 10Kh9K3V1M1FBR and their effect on the mechanical properties. *Met. Sci. Heat Treat.* **2010**, *52*, 100–110. [CrossRef]
35. Kim, H.K.; Lee, J.W.; Moon, J.; Lee, C.H.; Hong, H.U. Effects of Ti and Ta addition on microstructure stability and tensile properties of reduced activation ferritic/martensitic steel for nuclear fusion reactors. *J. Nucl. Mater.* **2018**, *500*, 327–336. [CrossRef]
36. Mythili, R.; Saroja, S. Influence of Tungsten and Tantalum Content on Evolution of Secondary Phases in 9Cr RAFM Steels: An Experimental and Computational Study. *Metall. Mater. Trans. A* **2017**, *48*, 3880–3891. [CrossRef]